Self-organized symmetry-breaking current filamentation and multistability in Corbino disks

G. Schwarz, C. Lehmann, and E. Schöll
Institut für Theoretische Physik, Technische Universität Berlin, Hardenbergstraße 36, D-10623 Berlin, Germany
(Received 29 September 1999)

A complex symmetry-breaking current instability in doped semiconductors induced by low-temperature impact ionization breakdown is investigated. We present computer simulations revealing the dynamics of the self-organized formation of multiple current filaments in *n*-GaAs Corbino disks, i.e., samples with concentric circular contacts. Our results explain the nascence of a filament in terms of two consecutive stages: a radially symmetric impact ionization front spreading from the inner contact becomes unstable and breaks up into a number of streamers evolving into prefilaments. With rising current, competition between those prefilaments takes place due to the global coupling via the load resistance. Only a small number of these survive and grow into fully developed filaments. Using the applied bias as a control parameter we find multistability and hysteresis, with jumps in the current-voltage characteristic caused by the spontaneous formation of additional filaments in the Corbino disk.

I. INTRODUCTION

Impact ionization of charged impurities is a key process in inducing current instabilities in semiconductors including self-generated current oscillations and chaos as first observed by Aoki[1] and Teitsworth *et al.*[2] Epitaxial semiconductor layers in the regime of low-temperature impurity breakdown have recently become a prominent model system for investigating self-organized nonlinear spatiotemporal patterns in a variety of geometries.[3] Semiconductor materials like *n*-GaAs at low temperatures exhibit an S-shaped current density-field relation due to impact ionization of carriers from shallow donors into the conduction band under high electric fields. It is known from various different physical systems that such S-shaped negative differential conductivity (SNDC) can give rise to the formation of current filaments[4] often displaying complex dynamic behavior.[5–9] For doped GaAs the occurrence and shape of such filaments has been studied extensively both experimentally and in computer simulations investigating thin-film samples with point contact geometries in the framework of phenomenological[10,11] and microscopic models.[12–14]

Sophisticated noninvasive measurement techniques such as quenched photoluminescence[15] or near-field scanning photoluminescence[16] have allowed us to map two-dimensional carrier density distributions, and thus spatially resolve filamentary structures. This has opened up the possibility to directly observe current filaments in *n*-GaAs thin films due to impact ionization of carriers from shallow donors. Moreover, it might also lead to new insights into the avalanche process of carrier excitations over the Landau gap[17,18] and current filamentaton[19–21] in quantum Hall effect breakdown.

Recently, current instabilities in samples with circular contact geometries, known as Corbino disks, have attracted interest by experimental groups.[22] Those Corbino disks mimic semiconductor samples without lateral boundaries by inducing current flow between a central point contact and a circular symmetric ring electrode. Thus they represent a versatile model system for investigating current filamentation in the absence of lateral boundary effects. Here, unlike in samples with point contacts, the occurrence of a current filament from a previously homogeneous or radially symmetric current density profile represents a symmetry-breaking instability. Such filamentary structures due to impurity breakdown in *n*-GaAs have been observed experimentally by spatially resolved quenched photoluminescence techniques.[22]

However, the origin of this symmetry-breaking filamentation and the observed hysteretic behavior associated with the spontaneous nascence of additional filaments, and its formation dynamics, remain unclear. It is the aim of this paper to explain the complex spatiotemporal dynamics of those spontaneous symmetry-breaking processes by detailed computer simulations within a microscopic model using Monte Carlo data on the nonequilibrium scattering processes as an appropriately parametrized input.

The organization of the paper is as follows. After a brief introduction of the model we present computer simulations of the formation process of a single filament at low bias voltage. Using the applied bias as a control parameter we then study the consecutive self-organized creation of additional filaments as the bias is increased; this is associated with multistability and hysteresis. Finally, we draw some conclusions.

II. MODEL

In this section we shall briefly summarize the model underlying our simulations.[23,12] We consider an *n*-doped semiconductor at liquid-helium temperature. The carrier density in the conduction band, $n(\mathbf{x},t)$, and hence the current density, is determined by the generation-recombination (GR) processes, including impact ionization of carriers between the conduction band and the donor levels. The experimentally observed S-shaped current density-field relation in the regime of impurity breakdown can be explained in terms of GR kinetics involving at least two impurity levels.[4] The GR cycle starts with impact ionization from the donor ground state, and is sustained at lower fields by impact ionization of much less strongly bound excited states, whose carrier concentrations are denoted by $n_1(\mathbf{x},t)$ and $n_2(\mathbf{x},t)$, respectively.

Our theoretical approach self-consistently combines Monte Carlo simulations of the microscopic scattering processes and GR kinetics with rate equations for the macroscopic spatiotemporal dynamics of the carrier densities, n, n_1, n_2, expressed through the continuity equations

$$\frac{\partial n}{\partial t}=\frac{1}{e}\nabla\cdot\mathbf{j}+\phi(n,n_1,n_2,|\mathcal{E}|),$$

$$\frac{\partial n_i}{\partial t}=\phi_i(n,n_1,n_2,\mathcal{E}),\quad i=1,2, \tag{1}$$

where e is the electron charge, ϕ, ϕ_1, ϕ_2 are the respective GR rates, $\mathcal{E}$ is the local electric field, and the current density $\mathbf{j}$ is given within the drift-diffusion approximation as $\mathbf{j}=e(n\mu\mathcal{E}+D\nabla n)$ with mobility μ and diffusion coefficient D.

In an explicit GR model[4] for low-temperature n-type GaAs, the transition rates between the levels ϕ, ϕ_i, which must satisfy $\phi+\phi_1+\phi_2=0$, are expressed by a set of nonlinear rate equations including thermal ionization of the excited level (rate coefficient X_1^S), capture of electrons into the excited level (T_1^S), relaxation (T^*), and excitation (X^*) between the excited and the ground levels, and impact ionization of the ground (X_1) and excited (X_1^*) levels. The impact ionization and capture coefficients that occur therein and that contain the essential nonlinear dependences upon the carrier densities and the field have been determined for n-GaAs by a single-particle Monte Carlo simulation.[24] Those GR coefficients are evaluated by averaging the microscopic transition probabilities over the nonequilibrium carrier distribution function $f(\boldsymbol{k})$, which is extracted from the MC simulation. Note that f, and hence the GR coefficients, depend parametrically on n, n_1, n_2, and $\mathcal{E}$. An iteration procedure, where n_1 and n_2 are expressed through (1) by their steady-state dependence on n and $\mathcal{E}$, is used to solve the above problem self-consistently.

It is possible to express the dependence of the GR coefficients upon $\mathcal{E}$ and n through the electron temperature $T_e(\mathcal{E},n)$.[23] Here we use the notion of electron temperature T_e in the usual sense of the mean electron energy $\frac{3}{2}k_BT_e=\langle E\rangle=(\hbar^2/2m)\langle k^2\rangle$, i.e., the electron temperature is extracted from the MC data essentially as the second moment of the nonequilibrium distribution function $f(\boldsymbol{k})$. This should not be confused with the concept of a heated Maxwellian distribution function, where the electron temperature appears as a parameter. This latter concept is much more restrictive since it assumes a quasithermal equilibrium of the conduction band subsystem. The MC data yield a strong increase of T_e with rising electric field on the high-conductivity branch of the current-voltage characteristics as opposed to only a slight increase on the low-conductivity branch. The strong increase is associated with a population inversion between the donor ground and the excited state on the upper branch.[12]

The local electric field is coupled to the carrier concentrations via Gauss' law

$$\epsilon\nabla\cdot\mathcal{E}=e(N_D^*-n_1-n_2-n), \tag{2}$$

where ϵ is the dielectric constant and $N_D^*\equiv N_D-N_A$ holds with the donor concentration N_D and the compensating acceptor concentration N_A. Finally, the total current through the sample $I=\int\mathbf{j}\cdot\mathbf{df}$ and the sample voltage $U=\int\mathcal{E}\cdot d\mathbf{x}$ between the two contacts must satisfy Kirchhoff's law

$$U=U_0-RI \tag{3}$$

with the load resistance R and the applied bias U_0. This represents a global constraint for the system (1), (2).

III. SIMULATIONS

For a given sample voltage U the electron distribution $n(\mathbf{x},t)$, $n_1(\mathbf{x},t)$, $n_2(\mathbf{x},t)$ and the electric field profile can be calculated self-consistently using Eqs. (1), (2). Since we consider thin-film samples we solve (1), (2), (3) on a two-dimensional spatial domain using an implicit finite-element scheme in space combined with a backward Euler scheme in time.[25] The two ohmic contacts are modeled by Dirichlet boundary conditions for the electron densities. An external voltage U_0 is applied via a load resistance of $R=10$ kΩ in an initial linear voltage ramp of 1 ps, after which it is kept constant.

We consider circular samples of radius 1.05 mm with concentric contacts. First, we apply an external bias of $U_0=2.05$ V to a sample with a small circular central contact of radius 0.04 mm such that this contact is the cathode, i.e., the injecting contact for majority carriers. Figure 1 shows the spatial profile of the current density in a logarithmic scale at different times t of the simulation. Equipotential lines are also shown. Initially, at $t=1$ ps we have a homogeneous nonconducting state, and the equipotential lines are concentric circles corresponding to a radial electric field decreasing with distance. Then a radially symmetric impact ionization front forms at the inner contact, where the electric field is highest due to the circular sample geometry [Fig. 1(a)]. The front moves towards the other contact, expanding in diameter. Note that the electric field behind the front is decreased due to the higher carrier density, i.e., lower resistance, such that almost all the voltage drop occurs in the nonconducting region outside the circular front. The equipotential lines indicate that the field is particularly high just ahead of the front, encouraging further downstream impact ionization and acceleration of the front. At about $t=0.15$ ns [Fig. 1(b)] the front spontaneously breaks up and evolves into five streamers of slightly different strength, each of which continues to expand towards the outer ring electrode [Fig. 1(c)]. This spontaneous symmetry-breaking instability can be understood by inspecting the equipotential line that approximately follows the contour of the front, corresponding to the interface between the conducting interior and the nonconducting exterior region. A small local perturbation of the front contour will result in a squeezing of the equipotential lines such that the field becomes highest at the point of maximum curvature. Therefore impact ionization will be enhanced there, and the bulge of the front will grow further, forming a streamer. Note that the streamer expansion is driven by the collective impact ionization process, and not by individual drifting carriers; it is about an order of magnitude faster than the carrier drift velocity (front velocity $v_f\approx 6\times10^5$ m/s, electron drift velocity $v_d\approx 5\times10^4$ m/s). Similar self-generated streamer instabilities of *planar* fronts have been known also in plasma physics.[26,27]

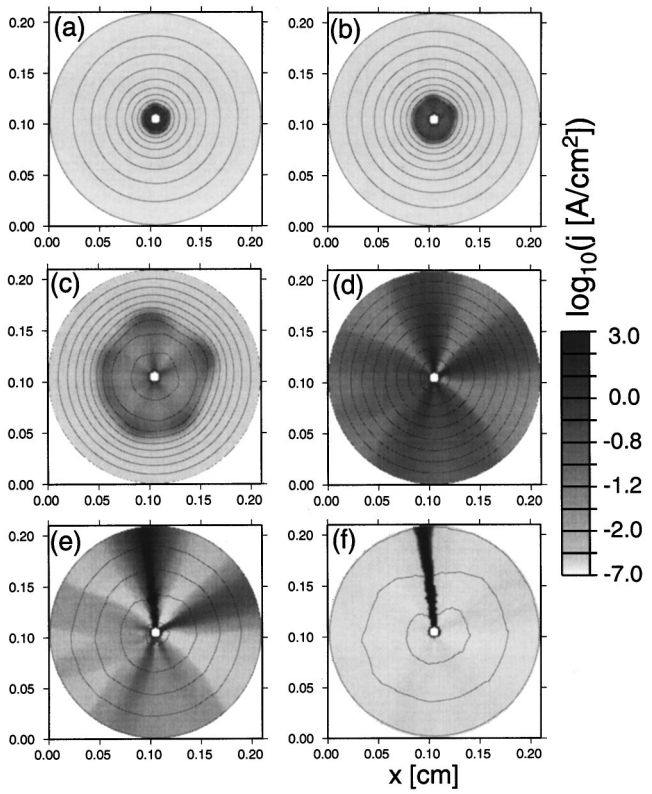

FIG. 1. Simulation of spontaneous symmetry-breaking current filament formation in an *n*-GaAs Corbino disk (inner radius $r_1 = 0.04$ mm, outer radius $r_2 = 1.05$ mm) upon application of a constant bias of $U_0 = 2.05$ V (center contact is cathode). The spatial distribution of the current density is depicted at different times (a) $t = 0.05$ ns, (b) $t = 0.15$ ns, (c) $t = 0.95$ ns, (d) $t = 5.15$ ns, (e) $t = 7.75$ ns, (f) $t = 20.00$ ns. Equipotential lines are plotted spaced by 0.2 V. The numerical parameters are the same as those used in Ref. 23 for simulations of rectangular *n*-GaAs samples with point contacts $N_D = 7\times10^{15}$ cm^{-3}, $N_A = 2\times10^{15}$ cm^{-3}, $\mu = 10^5$ cm^2/Vs, $\epsilon_r = 10.9$, $X_1^S = 1.17\times10^6$ s^{-1}, $X^* = 3.36\times10^3$ s^{-1}, $T^* = 4.1\times10^7$ s^{-1} ($R = 10$ kΩ, $T = 4.2$ K).

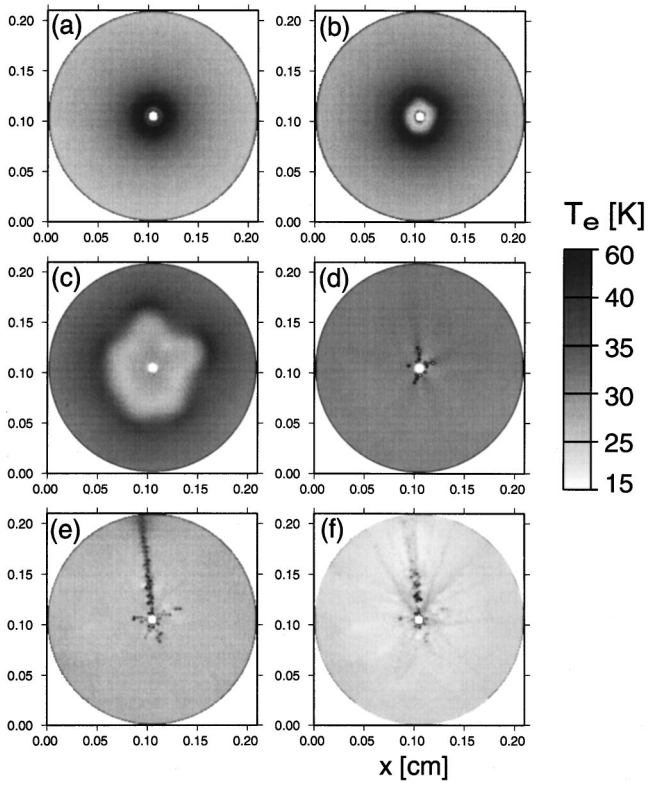

FIG. 2. Same as in Fig. 1, but for the electron temperature distribution.

Upon reaching the anode the streamers form prefilaments that subsequently grow in current density while approximately retaining their width [Fig. 1(d)]. This leads to a rising overall current I and thus, via the external load resistance, to a reduction in the sample voltage U due to the global constraint (3). This induces a competition between the prefilaments [Fig. 1(e)] and, eventually, to a winner-takes-all dynamics, which leaves as a fully developed current filament only the one that has first reached the outer contact. The remaining prefilaments slowly decay into the nonconducting state on the time scale of electron capture and subsequent relaxation into the donor ground state [Fig. 1(f)], which is the slowest process in the GR cycle. Figure 2 shows the evolution of the electron temperature distribution $T_e(\mathbf{x},t)$ for the same parameters. T_e is highest in the high-field region ahead of the expanding front, and decreases behind it because the field is lower there and because impact ionization leads to substantial cooling of the electron gas.[24]

In the simulation depicted in Fig. 3 the bias voltage is reversed, i.e., the inner electrode is now the anode. Again an impact ionization front spreads from the inner contact although this is now the noninjecting contact [Fig. 3(a)]. The reason is that the front is triggered by impurity impact ionization in the high-field region near the small central circular contact. It quickly breaks up into a number of streamers [Fig. 3(b)]. In this case the propagation of the streamers and the growth in current density is much faster than in Fig. 1 [Fig. 3(c)]. This is due to the initially stronger field in the depleted high-resistivity zone near the blocking central anode contact that strongly enhances impact ionization during the early stages. Additionally, the increased electron density near the injecting ring contact facilitates the rapid punch through of those streamers that are slightly ahead of the others [Fig. 3(d)]. As a result, small differences are strongly enhanced, and one obtains sharper streamer profiles than for positive bias. The subsequent competition due to the global coupling via R eventually leads to a single remaining filament, as before in the case of positive bias [Fig. 3(e)]. The electron temperature distribution (Fig. 4) also reveals a more distinct decrease behind the front due to much lower fields, as compared to positive polarity. The field is very efficiently screened by the impact ionized carriers.

Figure 5 depicts the total current as a function of time for both polarities. It can be seen that although the velocity of the streamers is more than twice as fast for negative U_0 and the current rises much more rapidly, the basic mechanism of filament formation out of the radially symmetric initial state is the same in both cases. The different stages of streamer motion and growth of filaments are clearly distinguished.

Next, we vary the bias voltage and investigate how the stationary spatial current density patterns change upon increase of the total current. To this end we sweep the bias U_0 from 1.0 V to 150.5 V in steps of 0.5 V, allowing the system to relax to a stationary filamentary state for 20 ns between

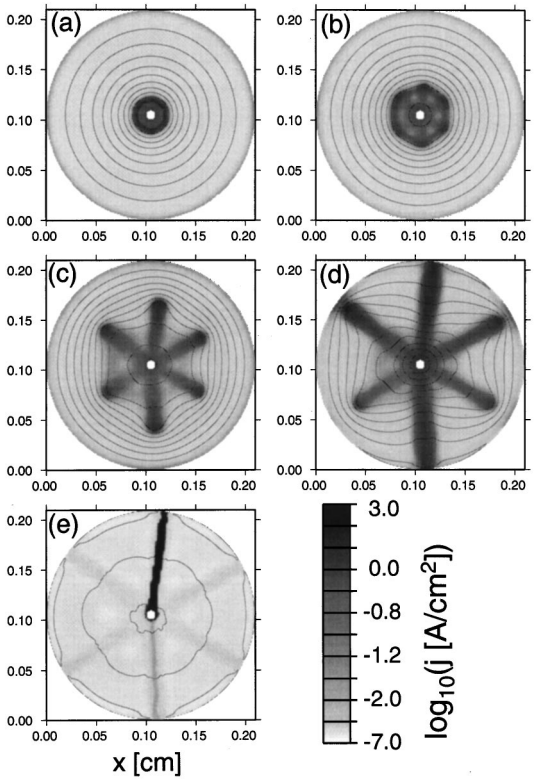

FIG. 3. Nascence of a current filament in an *n*-GaAs Corbino disk for $U_0 = -2.05$ V (center contact is anode). The spatial distribution of the current density is depicted at different times (a) $t = 0.15$ ns, (b) $t = 0.35$ ns, (c) $t = 0.75$ ns, (d) $t = 1.00$ ns, (e) $t = 20.0$ ns. Equipotential lines are plotted spaced by 0.2 V. Numerical parameters as in Fig. 1.

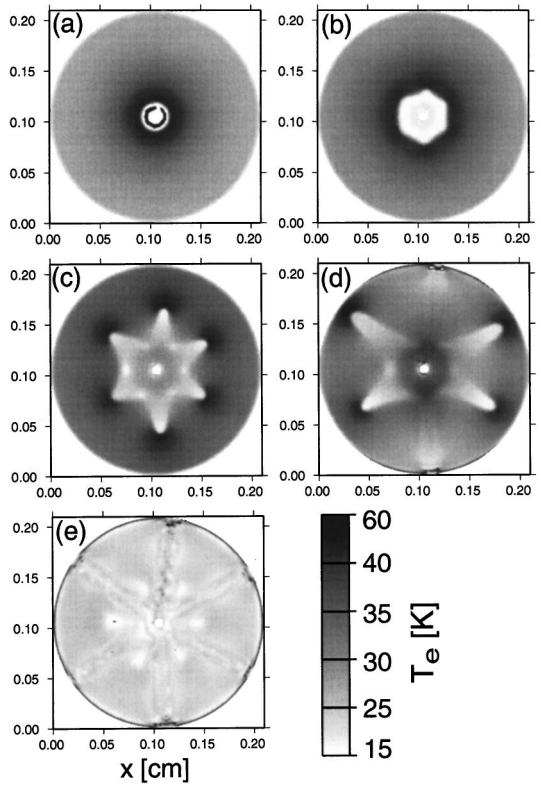

FIG. 4. Electron temperature distributions corresponding to Fig. 3.

each bias step. We consider a concentric Corbino sample with an outer radius of 1.05 mm and an inner radius of 0.25 mm and use the inner contact as cathode. At $U_0 = 150.5$ V we reverse the bias sweep direction, decreasing it again in steps of -0.5 V. The main diagram of Fig. 6 shows the total current I vs the voltage drop at the sample U. The arrows denote the sweep direction. The spatial distribution of the current density is depicted for different operating points on the current-voltage characteristic, given by the intersection of the load line, Eq. (3), and the $I(U)$ characteristic. The characteristic consists of consecutive discontinuous branches, each of which is associated with a specific number of current filaments. As the bias voltage U_0 is increased, the load line, which is almost horizontal for the value of $R = 10$ kΩ chosen, is shifted parallel and the operating point moves up on the lowest branch corresponding to a homogeneous nonconducting state [Fig. 6(a)]. At a threshold voltage $U \approx 1.3$ *V* (corresponding to about 16 V/cm, if one assumes a linear voltage drop) this state becomes unstable, and upon further increase of U_0 the operating point jumps to the branch [Figs. 6(b)–6(d)], which corresponds to a single fully developed filament. The simulation of the nascence of a filament in Fig. 1 was performed in this regime. Between Figs. 6(b) and 6(c) the filament width and the current remain almost the same, and only the internal field grows. If U_0 is increased from $U_0 = 11.5$ V, Fig. 6(d), by one further bias step, an additional filament forms, Fig. 6(e), and the total current I distinctly increases. Hence the sample voltage $U = U_0 - RI$ drops sharply, reaching the lower end of a new branch in the $I(U)$ characteristic. The internal field relaxes to a lower, almost homogeneous value visualized by essentially equidistant equipotential lines. Note that for U_0 slightly below this threshold the ''ghost filament'' is already visible in the logarithmic current density plot Fig. 6(d). Upon further increase of U_0 successive branches with three, Fig. 6(f), and four, Fig. 6(g), filaments are reached in the current-voltage characteristic on similar arguments. The jumps occur when

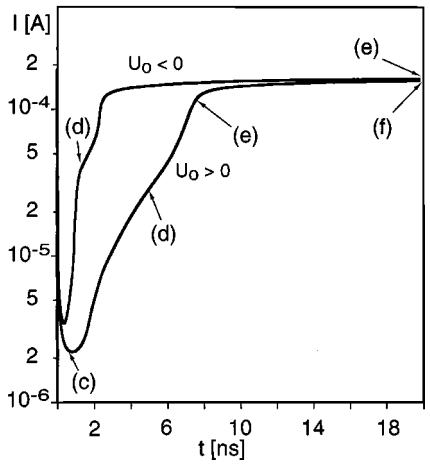

FIG. 5. Total current I vs time t during the formation of a current filament in a Corbino disk for different polarities of the applied bias: center contact is cathode (full line) or anode (broken line). The letters correspond to the current density profiles depicted in Figs. 1 and 3, respectively. Numerical parameters as in Fig. 1.

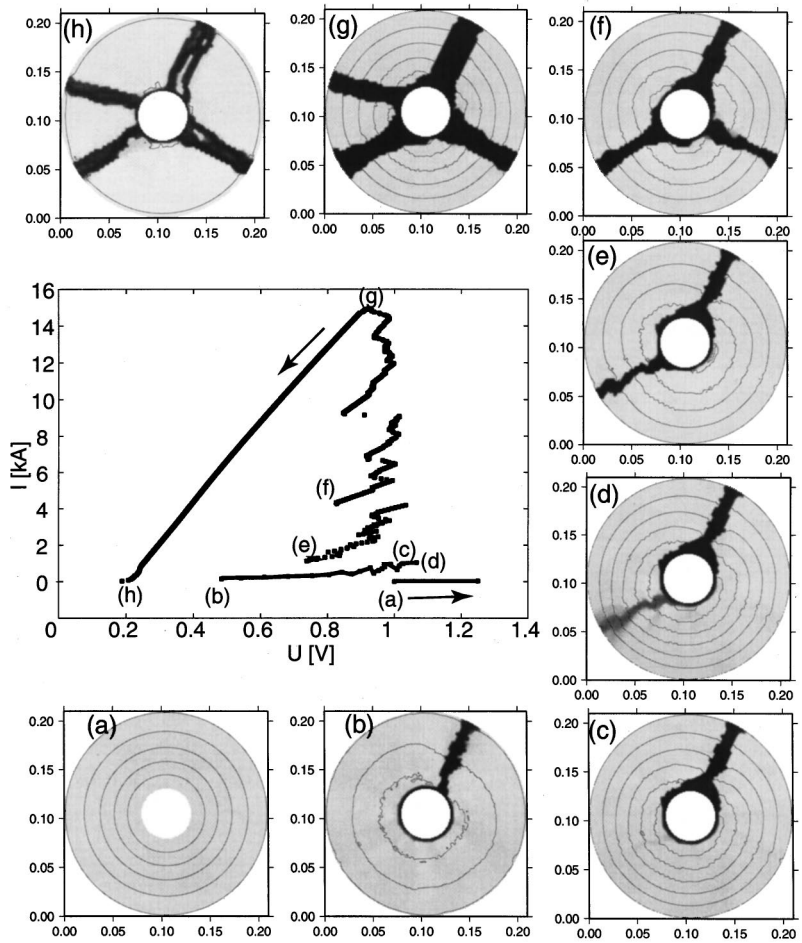

FIG. 6. Voltage sweep (up and down) of an *n*-GaAs Corbino disk. Main figure: global current-voltage characteristic. Side figures: spatial current density distribution for different operating points on the $I(U)$ characteristic: (a) external bias $U_0=1$ V, (b) $U_0=2$ V, (c) $U_0=11$ V, (d) $U_0=11.5$ V, (e) $U_0=12$ V, (f) $U_0=43.5$ V, (g) $U_0=150.5$ V, (h) $U_0=1.5$ V. The same logarithmic scale as in Figs. 1, 3 for the current density is used. Equipotential lines are plotted spaced by 0.2 V. Numerical parameters as in Fig. 1. The arrows indicate the bias sweep direction.

the internal field becomes so high that an additional filamentary channel (streamer) breaks through at a different location. The small discontinuities that can be observed within the branches are related to changes in the detailed shape of a filament, particularly at the contacts, which results in a change of the overall current and thus of sample voltage.

For bias downsweep we observe hysteretic behavior. The four stable current filaments, Fig. 6(g), e.g., persist for much lower U_0, Fig. 6(h), than the bias where they have first occurred. This is explained by the holding field of impact ionization that is generally much less than the threshold field.[4] The current density I decreases linearly with voltage U, which means that the sample conductance determined essentially by the carrier density in the filaments remains constant as long as the field does not fall below the holding field. By appropriate downsweeps starting from different branches of the characteristic a large number of multistable states corresponding to different numbers of filaments can be reached for a given bias U_0. Thus this system exhibits a high degree of self-organized multistability.

IV. CONCLUSIONS

Our simulations of nonlinear transport in a Corbino geometry with two concentric circular contacts have revealed a spontaneous symmetry-breaking instability that explains the origin of the formation of stationary current filaments observed experimentally in thin-film *n*-GaAs Corbino samples[22,28] in the regime of low-temperature impurity breakdown. We find that this instability occurs as a two stage process.

First, upon application of a dc bias via a load resistance a radially symmetric impact ionization front spreads from the central contact. This process is always initiated, regardless of the bias polarity, at the central contact due to the higher electric field there, even if this is the noninjecting anode. As the impact ionization front expands towards the outer ring contact, it becomes unstable against azimuthal fluctuations and breaks up into a number of fast streamers, thus spontaneously breaking the radial symmetry of the system. When the streamers reach the ring contact they form prefilaments whose current density is still several orders of magnitude lower than that of a fully developed current filament. The formation process of the prefilaments, whose physical mechanism is very similar to the initial stage of the nascence of a single current filament in a sample with two point contacts,[13] occurs on a subnanosecond time scale. If the central contact is noninjecting, the process is even considerably faster due to larger fields and hence strongly increased impact ionization.

In the second stage, the current density of the prefilaments rises due to impurity impact ionization, sharply increasing the overall current. Due to the external load resistance, which represents a global coupling of the individual filaments via the total current I, an increase of the current in any of the filaments results in a reduction in the sample voltage U and thus in the average field in each filament. This mechanism leads to a winner-takes-all dynamics, where small initial differences between the filaments are enhanced, and, for small enough total current, eventually only one filament survives while the others decay, albeit on a slower time scale due to the slow recombination processes.

For larger total current, i.e., higher applied bias voltage U_0, stable spatial patterns with two and more filaments occur. With growing voltage, the filaments essentially retain their size. If the field exceeds a threshold, an additional filament is created at a different location in another symmetry-breaking instability. This has been demonstrated by sweeping the bias voltage over a larger range such that, e.g., up to four filaments are successively created. Because of the series load resistance, each increase in the number of filaments and hence increase of the overall current I is associated with a jump on the $I(U)$ characteristic down to smaller sample voltages U. Therefore the $I(U)$ characteristic consists of a sequence of discontinuous branches corresponding to different numbers of filaments. Reversing the bias sweep direction we find hysteresis because the sustaining voltage is substantially lower than the threshold voltage. Thus the Corbino sample represents a highly multistable system, and various multiple filament states can be reached at the same bias voltage by appropriate sweeps. This multistability has an advantage over the multistable filamentary current-voltage characteristics, which have been realized by arrays of point contacts in rectangular n-GaAs samples,[29] since in our case the multiple filaments arise in a self-organized way and do not need complicated structuring of multiple point contact geometries. Switching between different multifilamentary states in those structures has been discussed in the context of data storage and synergetic computers. Other semiconductor systems where multistable spatial patterns have attracted interest because of their potential prospects as multibit memory elements include field domains in semiconductor superlattices.[30]

It should be noted that our simulations do not involve any intentionally introduced inhomogeneities or perturbations of the radial symmetry of the sample geometry or of the initial conditions. The minute, inevitable numerical inaccuracies introduced by the algorithm and the discretization grid are sufficient to trigger the spontaneous symmetry-breaking instability of the radial front. Thus small numerical discrepancies among different computer architectures can lead to different azimuthal positions of the final, fully developed filaments for nominally identical simulations, as do unavoidable inhomogeneities and fluctuations in real physical systems. The principal occurrence of the consecutive multiple filamentation, however, is independent of numerics.

Our findings are in good agreement with recent experiments on n-GaAs Corbino disks,[22,28] where a sequence of successively generated filaments at increasing bias, associated with different current-voltage branches, and multistability due to a distinct hysteresis effect with respect to bias sweep up and sweep down have been directly observed by spatially resolved quenched photoluminescence. Our simulations cannot only explain these observations and give additional insight into the internal structure of these filamentary states by calculating, e.g., the electron temperature and electric potential distributions, but also explore the dynamic process of their formation that is not yet accessible experimentally due to the short time scales involved. In particular, we have resolved the question if a second filament arises by splitting of the existing filament, or by an independent symmetry-breaking process, which has been controversially discussed previously.[22]

ACKNOWLEDGMENTS

The authors would like to thank K. Aoki, J. Hirschinger, F.-J. Niedernostheide, V. Novák, and W. Prettl for fruitful discussions as well as H. Gajewski and R. Nürnberg for providing the TESCA package. Funding by Deutsche Forschungsgemeinschaft through Sfb 555 is acknowledged.

[1] K. Aoki, T. Kobayashi, and K. Yamamoto, J. Phys. Soc. Jpn. **B 51**, 2372 (1982).

[2] S. W. Teitsworth, R. M. Westervelt, and E. E. Haller, Phys. Rev. Lett. **51**, 825 (1983).

[3] V. V. Bel'kov, J. Hirschinger, V. Novák, F.-J. Niedernostheide, S. D. Ganichev, and W. Prettl, Nature (London) **397**, 398 (1999).

[4] E. Schöll, *Nonequilibrium Phase Transitions in Semiconductors* (Springer, Berlin, 1987).

[5] F.-J. Niedernostheide, C. Brillert, B. Kukuk, H.-G. Purwins, and H.-J. Schulze, Phys. Rev. B **54**, 14 012 (1996).

[6] F.-J. Niedernostheide, J. Hirschinger, W. Prettl, V. Novák, and H. Kostial, Phys. Rev. B **58**, 4454 (1998).

[7] V. Novák, J. Hirschinger, F.-J. Niedernostheide, W. Prettl, M. Cukr, and J. Oswald, Phys. Rev. B **58**, 13 099 (1998).

[8] E. Schöll, F.-J. Niedernostheide, J. Parisi, W. Prettl, and H. Purwins, in *Evolution of Spontaneous Structures in Dissipative Continuous Systems*, edited by F. H. Busse and S. C. Müller (Springer, Berlin, 1998), pp. 446–494.

[9] F. J. Niedernostheide and M. Kleinkes, Phys. Rev. B **59**, 7663 (1999).

[10] V. Novák, C. Wimmer, and W. Prettl, Phys. Rev. B **52**, 9023 (1995).

[11] V. Novák, J. Hirschinger, W. Prettl, and F.-J. Niedernostheide, Semicond. Sci. Technol. **13**, 756 (1998).

[12] M. Gaa, R. E. Kunz, and E. Schöll, Phys. Rev. B **53**, 15 971 (1996).

[13] M. Gaa, R. E. Kunz, E. Schöll, W. Eberle, J. Hirschinger, and W. Prettl, Semicond. Sci. Technol. **11**, 1646 (1996).

[14] K. Kunihiro, M. Gaa, and E. Schöll, Phys. Rev. B **55**, 2207 (1997).

[15] W. Eberle, J. Hirschinger, U. Margull, W. Prettl, V. Novák, and H. Kostial, Appl. Phys. Lett. **68**, 3329 (1996).

[16] I. Bar-Joseph, invited talk, HCIS-11 (Kyoto 1999) (unpublished).

[17] S. Komiyama, Y. Kawaguchi, T. Osada, and Y. Shiraki, Phys. Rev. Lett. **77**, 558 (1996).
[18] I. I. Kaya, G. Nachtwei, K. von Klitzing, and K. Eberl, Phys. Rev. B **58**, R7536 (1998).
[19] Ch. Simon, B. B. Goldberg, F. F. Fang, M. K. Thomas, and S. Wright, Phys. Rev. B **33**, 1190 (1998).
[20] V. Tsemekhman, K. Tsemekhman, C. Wexler, J. H. Han, and D. J. Thouless, Phys. Rev. B **55**, R10 201 (1997).
[21] L. Eaves, Physica B **256**, 47 (1998).
[22] J. Hirschinger, W. Eberle, W. Prettl, F.-J. Niedernostheide, and H. Kostial, Phys. Lett. A **236**, 249 (1997).
[23] M. Gaa, R. E. Kunz, and E. Schöll, in *Proceedings of the 9th International Conference on Hot Carriers in Semiconductors*, edited by K. Hess, J. P. Leburton, and U. Ravaioli (Plenum, New York, 1996), pp. 347–351.
[24] B. Kehrer, W. Quade, and E. Schöll, Phys. Rev. B **51**, 7725 (1995).
[25] R. E. Kunz, E. Schöll, H. Gajewski, and R. Nürnberg, Solid-State Electron. **39**, 1155 (1996).
[26] U. Ebert, W. van Saarloos, and C. Caroli, Phys. Rev. Lett. **77**, 4178 (1996).
[27] U. Ebert, W. van Saarloos, and C. Caroli, Phys. Rev. E **55**, 1530 (1997).
[28] K. Aoki and S. Fukui, Physica B **272**, 274 (1999).
[29] H. Kostial, K. Ploog, R. Hey, and F. Böbel, J. Appl. Phys. **78**, 4560 (1995).
[30] J. Kastrup, H. T. Grahn, K. Ploog, F. Prengel, A. Wacker, and E. Schöll, Appl. Phys. Lett. **65**, 1808 (1994).